



JGR Atmospheres

RESEARCH ARTICLE

10.1029/2020JD032942

Special Section:

The Land-Air Coupling Over Tibetan Plateau and Its Global Climate Effects

Key Points:

- Dust-forced radiative heating (DRH) has a significant warming effect with the center from dust sources to adjacent transport regions
- The near-surface DRHs over the Tibetan Plateau and its surroundings (TPS) are 3–3.6 times larger than the column-averaged value
- Dust aerosols over the TPS may have the potential to exert more snow melting driven by the remarkable near-surface warming effect

Supporting Information:

- Supporting Information S1

Correspondence to:

J. Huang,
hjp@lzu.edu.cn

Citation:

Wang, T., Han, Y., Huang, J., Sun, M., Jian, B., Huang, Z., & Yan, H. (2020). Climatology of dust-forced radiative heating over the Tibetan Plateau and its surroundings. *Journal of Geophysical Research: Atmospheres*, 125, e2020JD032942. <https://doi.org/10.1029/2020JD032942>

Received 20 APR 2020

Accepted 28 JUL 2020

Accepted article online 3 AUG 2020

Author Contributions:

Conceptualization: Tianhe Wang, Jianping Huang

Data curation: Mengxian Sun, Bida Jian

Formal analysis: Tianhe Wang, Ying Han, Bida Jian

Investigation: Tianhe Wang

Methodology: Tianhe Wang, Ying Han, Mengxian Sun, Zhongwei Huang

Project administration: Jianping Huang

Software: Ying Han, Mengxian Sun, Zhongwei Huang

(continued)

©2020. American Geophysical Union.
All Rights Reserved.

Climatology of Dust-Forced Radiative Heating Over the Tibetan Plateau and Its Surroundings

Tianhe Wang¹ , Ying Han¹, Jianping Huang¹ , Mengxian Sun¹, Bida Jian¹, Zhongwei Huang¹, and Hongru Yan¹ 

¹Key Laboratory for Semi-Arid Climate Change of the Ministry of Education, College of Atmospheric Sciences, Lanzhou University, Lanzhou, China

Abstract Dust aerosol can affect the atmospheric thermal structure and exert great melting potential on snow and ice sheets. In this study, the decadal climatology of dust-forced radiative heating (DRH) in the atmosphere over Tibetan Plateau and its surroundings (TPS) was investigated using the Santa Barbara DISORT Atmospheric Radiative Transfer (SBDART) model along with the CALIPSO satellite observations from 2007 to 2016. After screening out other aerosols, the vertical distribution of dust aerosol was examined to accurately assess the DRH. The net DRH showed a significant warm effect mainly by dust loading, which covers from the center of dust sources to their adjacent transport regions. The maximum value of the DRH appeared at the near-surface, while the DRH decreased with an increase in height. The climatic average DRH at the near-surface reached 16.8 K/month at the Taklimakan Desert (TD) and 10.8 K/month at the Gangetic Plain in spring, 13.7 K/month at the Indus Plain in summer, which is 3–3.6 times warmer than the column-averaged DRHs. This study also found the most significant influence of dust events on the Qaidam Basin in the TPS, in which the near-surface DRH was 4.7 K/month during spring. It is also noteworthy that the intermonth and interannual variations of the DRH highlighted the significant warming effect of dust aerosols on the atmospheric thermal structure, especially at the near-surface. In addition, we need to pay more attention to changes in snow-related processes influenced by absorbing aerosols and the light-absorbing impurities deposited in snow over the TPS.

1. Introduction

The Tibetan Plateau (TP), known as the “third pole” of the world, has a crucial influence on the Asian monsoon system and Northern Hemispheric climatology as it has distinctive geographical and complex terrain features (Qiu, 2008; Yao et al., 2012; Zhou et al., 2014). The TP where the second largest glacier reserve of around 1,000,000 km² exists (Yao et al., 2019) is also called the “Water Tower of Asia” mainly as the Yangtze River, the Yellow River, the Lantsang River, and other important rivers originate from the TP (Chen et al., 2016). In the last few decades, the TP has suffered from considerable warming (Huang et al., 2012), resulting in a dramatic glacial decline (Kang et al., 2010). The changes in the atmosphere and the water cycle may induce alterations in the climate and environment at the local and adjacent areas (Cao et al., 2006; Yao et al., 2004). Consequently, the portion of arid and semiarid regions around the TP has been expanded at an accelerating rate (Huang et al., 2015), resulting in considerable contributing to desertification in Northern China (Liu et al., 2020). Therefore, many studies have paid attention to the increased surface and atmospheric heating that may be a primary driver of climate change in the TP.

As there are little population and industrial activities, the TP is one of the most pristine terrestrial regions outside the north and south poles (Wake et al., 1994). However, a number of studies have demonstrated that the TP has been exposed to polluted air masses containing the absorbing aerosol from the local and surrounding areas (Che et al., 2015; Huang, Minnis, et al., 2007; Liu et al., 2015; Ma et al., 2020; Wang et al., 2020). On one hand, these absorbing aerosols deposited in snow may not only reduce the surface albedo (Gautam et al., 2013; Yasunari et al., 2015) but also absorb the radiation that drives the snow surface warmer. Consequently, the absorbing aerosols deposited in snow cause accelerated snow melting which affects the cryosphere (Flanner et al., 2009; Shi et al., 2019). On the other hand, the absorbing aerosols floating in the atmosphere can directly influence the net radiation between atmosphere and surface by absorbing and scattering solar radiation as well as interacting with terrestrial long-wave radiation (Che, Gui, et al., 2019), subsequently resulting in great impacts on the thermal structure (Wonsick et al., 2014) and

Supervision: Jianping Huang

Visualization: Ying Han

Writing - original draft: Tianhe

Wang, Ying Han

Writing - review & editing: Tianhe

Wang, Jianping Huang, Hongru Yan

snow melting in the plateau (Lau et al., 2010; Painter et al., 2018). Absorbing aerosols also contribute to large diabatic heating in the atmosphere, enhancing cloud evaporation (Huang et al., 2006; Wang & Huang, 2009). Besides, the absorbing aerosols also influence the cloud properties and climate by acting as cloud condensation nuclei and ice nuclei (Huang et al., 2014; Yan & Wang, 2020). In this light, the absorbing aerosols play an important role in changing the climate and environment of the TP.

Recently, there is a growing recognition that a dominant absorbing aerosol type above the TP is dust (Wang et al., 2020; Xu et al., 2015) that may be sourced from the several areas around the TP such as the Taklimakan desert and the Thar Desert (Guo et al., 2017; Huang et al., 2008). Therefore, it is essential to understand the impacts of the dust-forced radiative heating on the atmosphere over the TPS. Recently, many studies have paid attention to investigating the mechanism of the dust aerosol and its impacts on the atmospheric thermal structure over the TPS. Lau et al. (2006) display the aerosol direct forcing on the atmosphere-land system over the TP using the Goddard Chemistry Aerosol Radiation and Transport (GOCART) model. They found that the dust aerosol over TP produces atmospheric dynamical feedback by heating midtroposphere, the so-called elevated heat-pump effect, which increases moisture, cloudiness, and deep convection over northern India. Lau et al. (2010) also found that dust aerosol enhances the rate of snowmelt in the Himalayas and TP. Chen et al. (2013) showed using the WRF-Chem model that a dust storm case can break through the planetary boundary layer and lift into the upper troposphere over the northern TP, which can even warm the atmosphere by 0.11 K/day at ~7 km. Although model simulations can provide fundamental information to understand the impacts and mechanism of the dust on the atmosphere over the TPS, there are considerable uncertainties that may be induced by aerosol optical properties and vertical distributions (Chen et al., 2014; Konsta et al., 2018).

The Cloud-Aerosol Lidar and Infrared Pathfinder Satellite Observations (CALIPSO), launched in April 2006, provides more accurate information on sensed vertical structures of aerosols (Z. Liu et al., 2008; D. Liu et al., 2008; Yu et al., 2010). Huang et al. (2009) found that dust aerosols induce heating the atmosphere (daily mean) by up to 1, 2, and 3 K/day in the light, moderate, and heavy dust layers, respectively, based on the Fu-Liou radiation model that incorporates the vertical distribution of dust aerosol from CALIPSO. Furthermore, it is necessary to examine the climatology of dust-forced radiative heating (DRH) to better understand the effects of dust aerosol on atmospheric thermal structure and snow melting. Employing the decadal vertical distribution of the dust aerosol obtained from CALIPSO from 2007 to 2016 into a radiative transfer model, this study estimated the climatology of DRH with constraints conditioned by other satellite observations and reanalysis data sets. The paper is organized as follows. All data sets and methods are introduced in section 2. Sections 3.1 and 3.2 provide analyses of the decadal climatology of extinction properties and the DRH over the TPS. The evolution and possible uncertainties of the DRH over TPS are discussed in section 3.3 and 3.4. The conclusions and discussions are presented in section 4.

2. Data Sets and Method

2.1. Total Dust Aerosol Extinction Coefficient Profiles

The dust and polluted dust aerosol profiles of the CALIPSO version 4 level 2, covering a 10-year period from 2007 to 2016, at a nominal resolution of 5 km along the track and vertical resolution of 60 m in the troposphere were used in this study. For high confidence data, this study selected only nighttime data with a cloud-aerosol discrimination (CAD) score between -70 and -100 not only to avoid the interference of sunlight during the day but also to ensure the right classification of dust and polluted dust aerosol layer features (Liu et al., 2019). The extinction quality control flag (Ext_QC) values of 0, 1, 2, 18, and 16 were selected to remove problematic retrievals for dust and polluted dust aerosols (Winker et al., 2013).

However, it is noteworthy that the backscatter/extinction coefficients of polluted dust may be contaminated by nondust aerosols. Thus, this study derived a ratio of dust to total backscatter (f_d) at each bin for each profile in order to remove the contribution of nondust aerosols as follows (Hayasaka et al., 2007):

$$f_d = \frac{(\delta - \delta_{nd})(1 + \delta_d)}{(1 + \delta)(\delta_d - \delta_{nd})} \quad (1)$$

where δ is the particulate depolarization ratio (PDR) retrieved by CALIPSO, δ_d and δ_{nd} are the prior knowledge of PDR for dust and nondust aerosol, respectively. According to previous studies that

Table 1
Descriptions of the Input Parameters of SBDART

Input	Data sets	Units
Surface spectral albedo	MODIS (BRDF/Albedo) Products (MCD43C3)	—
Temperature profile	ERA-Interim	K
Water vapor profile	MERRA-2 & ERA-Interim	g/m ³
Ozone density profile	OMO3PR	g/m ³
Column moisture content	ERA-Interim	g/cm ²
Column ozone content	OMO3PR	ATM-cm

observed the PDR (~ 0.31) for pure dust (Freudenthaler et al., 2017; Sugimoto et al., 2002), the PDR for the dust aerosol is always larger than that for nondust aerosols (Huang et al., 2020). Although the marine aerosol and urban haze are highly hygroscopic and generally have low PDR, specific nondust aerosols, such as biomass-burning smoke, sea-salt crystals, and ammonium sulfate, have a nonnegligible PDR of up to 0.07 (Yu et al., 2015). Luo et al. (2015) found that a PDR threshold of 0.075 can cause an unnecessary exclusion of dust events, while a low PDR below the threshold can induce an unintended inclusion of nondust cases. In this regard, the δ_{nd} in this study was assumed as 0.05 to avoid the unnecessary exclusion or inclusions of dust events. The value of f_d was set to 1 if $f_d > 1$ or for dust bins while it was set to 0 if $f_d < 0$ or for other aerosol types. The dust backscatter coefficient can be obtained from the product of the total backscatter and the calculated f_d . Afterward, the profiles of total dust extinction coefficient (DEC) were derived from the recalculated dust backscatter coefficient and an assumed dust extinction to backscatter ratio (lidar ratio; LR) of 44 at 532 nm as in previous studies (Kim et al., 2018). In this study, monthly mean values of the dust aerosol optical depth (DOD) and DEC were derived at $2^\circ \times 2^\circ$ resolution by the single aerosol species regrid average approach that assigned extinction as 0.0 km^{-1} for all other species prior to calculating the average dust extinction within a grid. This method can avoid a high bias in the averaged extinction at altitudes dominated by other aerosol species (Amiridis et al., 2013) and accurately represent the climatic characteristics of dust aerosol at each grid or regional scale by the recalculated dust distribution.

2.2. The SBDART Model

The Santa Barbara DISORT Atmospheric Radiative Transfer (SBDART) model (Ricchiazzi et al., 1998) was employed in this study to estimate the DRH over the TPS at the shortwave (SW: 0.25–4.0 μm) and longwave (LW: 4–80 μm) wavelengths. Table 1 shows the atmospheric background parameters that are interpolated to $2^\circ \times 2^\circ$ grid cells for matching the above gridded DOD in the SBDART model. Besides, the DEC profiles at 532 nm were directly derived from CALIPSO.

Important input parameters in the SBDART model are the single scattering albedo (SSA) and asymmetry factor (g) of the dust aerosol that are dependent on dust aerosol type. To optimize these two parameters over the TPS, as the work of Huang et al. (2009), we compared the instantaneous SW and LW radiative fluxes at the top of atmosphere (TOA) between observations of the Cloud and the Earth's Energy Budget Scanner (CERES) and simulations driven by the CALIPSO orbit with four dust aerosol types of the Optical Properties of Aerosol and Cloud (OPAC) package as shown in Table 2 (Hess et al., 1998). This study selected two typical pure dust cases that are located in the TD and the Thar Desert (ThD), respectively (refer to supporting information Figure S1 for the details). We found that the SSA and g of transported mode dust aerosol performed the best. Figure 1 shows a comparison of SW and LW flux the TOA between SBDART simulations and the CERES measurements along the CALIPSO orbit over the TD region (37°N – 40°N) for the daytime of 19 April 2012 and over the ThD region (22°N – 26°N) for the daytime of 27 April 2008. As the average differences in the SW and LW wavelength are only 28 and 12 W/m^2 , respectively, SSA and g of the transported dust mode were used in the following simulations. Uncertainty in the DRH driven by the assumption of transported mode over the TPS is further evaluated in section 3.4.

2.3. Calculation and Revision of the DRH

The DRH in the atmosphere mainly depends on the absorption of solar radiation by the dust aerosol (Huang et al., 2009). The climatology of DRH over the TPS is thus only evaluated during the daytime. Campbell et al. (2012) found that the mean aerosol optical depth (AOD) and the effective layer heights retrieved by CALIPSO during the nighttime were slightly lower or compatible compared to those during the daytime, indicating that the nighttime CALIPSO-driven aerosol products are reasonably consistent with daytime retrievals. Therefore, the nighttime DEC with high confidence was employed to examine the characteristics of the dust aerosol. The DRH is usually determined by the sum of the difference of SW and LW wavelengths between dust-laden and dust-free conditions (Peris-Ferrús et al., 2017). However, the radiative heating rate simulated by the SBDART model along the CALIPSO orbit only represents an instantaneous dust heating at

Table 2
Single Scattering Albedo (SSA) and Asymmetry Factor (g) for Four Dust Aerosol Types of the OPAC Package

	Nucleation mode	Accumulation mode	Transported mode	Coarse mode
SSA	0.9767	0.9203	0.89	0.7266
g	0.6471	0.7143	0.7460	0.8613

a 13:30 local time. Therefore, the daily mean DRH needs to be corrected from instantaneous one to consider the diurnal variation of the solar radiation by multiplying a normalized factor as follows:

$$DRH = (H_{SW}^{dust} - H_{SW}^{clear}) \cdot f + (H_{LW}^{dust} - H_{LW}^{clear}) \quad (2)$$

$$f = \frac{h_0 \sin(\varphi) \sin(\delta) + \cos(\varphi) \cos(\delta) \cos(h_0)}{\pi \sin(\varphi) \sin(\delta) + \cos(\varphi) \cos(\delta) \cos(h)} \quad (3)$$

where H_A^B is the instantaneous DRH of A (SW or LW) wavelength under a B condition (dust or clear), f is the normalization factor defined as the ratio of the daily mean flux density of solar radiation and the instantaneous one at some local solar time (Haynes et al., 2013), which takes into account the diurnal variation of insolation at each grid. Equation 3 is a specific definition based on the combination of inverse-square law, Lambert's cosine law, and spherical law of cosines (Johansson et al., 2015), where φ is the latitude, δ is solar declination of each grid, and h and h_0 are the angles at 13:30 local solar time and the sunrise at each grid, respectively.

Considering the geometry of CALIPSO lidar, there are sparse-frequency observations within a study domain, which makes it difficult to extract the climatology of dust aerosol extinction and even heating rate at a daily scale. Thus, this study rescaled to the monthly DEC values at each grid and the corresponding monthly cumulative DRH was calculated to represent the climatology of the DRH with a unit of K/month over the TPS.

3. Results

The TP is known as “Asian Water Tower” on the roof of the world, owning the greatest areas of snow cover and ice sheet in the world besides the polar region (Yao et al., 2019). The TP has suffered from considerable dust loadings from potential local and remote dust sources due to the combined influence of climate and topography (Jia et al., 2015). These dust aerosols are absorbing solar radiation, causing the potential effect on the atmospheric thermal structure, snow melting, and glacier retreat. Figure 2 shows the location of the TD, the TP, and the Indo-Gangetic Plain (IGP). Based on climate and potential dust sources, the TP (here defined as the altitude above 2,500 m) is subdivided into the western (TP_R1), the Qaidam Basin (TP_R2), and the southeastern (TP_R3). In addition, the IGP is also divided into the Indus Plain (IP) and the Gangetic Plain (GP) based on the border between Pakistan and India at the north of 23°N.

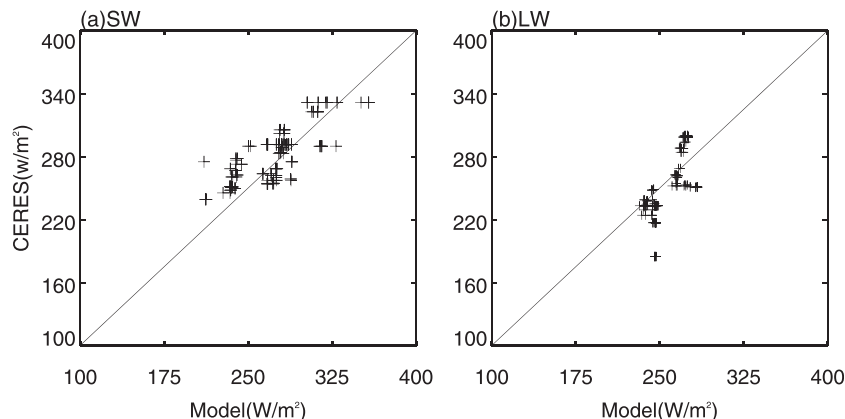


Figure 1. Comparison of instantaneous (a) SW and (b) LW radiative fluxes at the TOA between the model simulations and the CERES observations along the CALIPSO orbit over the TD region (37°N–40°N) on 19 April 2012 and ThD region (22°N–26°N) on 27 April 2008.

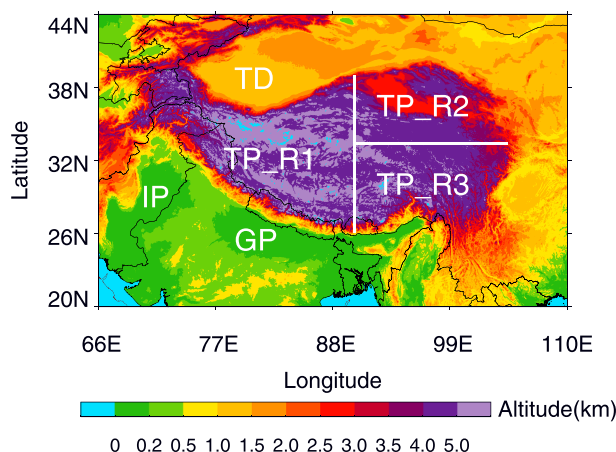


Figure 2. The topographical distribution and subregions in the TPS.

On the contrary to the previous studies that only incorporated dust events, this study recalculated the DOD with the single aerosol species regrid average approach to better reflect the climatic characteristics of the dust aerosol extinction.

Although the TP is the cleanest area in the TPS as shown in Figure 3, Figure 3 also showed considerable spatial and temporal variations of the DOD mainly due to the influence of dust aerosol from local and remote sources. For example, the peak DOD always occurred in the TP_R2 through the year due to the emission of abundant dust in the Qaidam Basin. Previous studies have demonstrated that frequent dust storms mainly contribute to an increase in the DOD over the Qaidam Basin (Pullen et al., 2011; Xu et al., 2015). Additionally, it is noticeable that prominent accumulations of dust aerosol were found at the southern and northern edges of the TP especially during MAM and JJA, which was also observed in the extinction coefficient profiles of dust aerosols in section 3.1.2. The lowest DODs occurred in the inland of the TP_R1 and TP_R3 except for MAM. A gradient distribution of DOD is also related to a topographical characteristic that there are mountains along the east-west in the TP as a barrier for the north-south transport of aerosols (Xu et al., 2014).

3.1.2. Vertical Distribution

Figure 4 illustrates the climatological vertical distribution of the decadal mean of the DEC at longitudinal (over 27°N and 39°N) and latitudinal (over 70°E, 81°E, and 93°E) cross-sections during MAM and JJA. Dust emission and loading were consistently larger at the dust source regions and gradually descending corresponding to transport processes (Liu et al., 2012). Besides, the extinction also decreased considerably with an increase in altitude. As the TP acts as a large natural barrier for the north-south transport of the dust aerosol from the TD and ThD, the dust vertical transport route can be altered from lower layers to higher layers, resulting in distinctly different vertical distributions of dust in the north and south of the TP. Over the TD, strong extinction (SE, $>0.1 \text{ km}^{-1}$) layers of the dust aerosol were extended to 3 km from the surface during MAM (Figures 4b and 4d) while diminishing or occurring only near the surface during JJA (Figures 4g and 4i). Given the intensification of the SAM and westward movement of the DOD peak center from GP to IP, the SE layer over the GP was contracted from 2 km in MAM (Figures 4a and 4d) to near the surface in JJA (Figures 4f and 4i). The SE layers over the IP during MAM and JJA were not changed significantly, the height of 2 km (Figures 4c and 4h). In contrast, the middle extinction (ME, $>0.01 \text{ km}^{-1}$) layers of dust aerosols over the TD, the GP, and the IP were extended to 6 km or even more.

The accumulations of dust aerosol on the southern and northern edges of the TP_R1 were observed in the longitudinal cross-section of 81°E as shown in Figures 4d and 4i. This result may be caused by the frequent convective updrafts that lift the dust aerosol over the TPS and retain an upward velocity during subsequent transport processes (Uno et al., 2009). Therefore, more dust aerosols are accumulated and transported to the northern edge of the TP from the TD than the southern TP, especially during MAM and JJA (Huang, Ge, et al., 2007). Although no significant dust plume transported from the IGP to the TP was observed by the CALIPSO satellite, a number of analyses on field samples in snow and glaciers over the TPS have verified

3.1. Climatology of Total Dust Extinction

3.1.1. Horizontal Distribution

Figure 3 shows the seasonal spatial distributions of the decadal mean of total DOD over the TPS. Overall, the spatial distributions are consistent with those in the previous satellite observations (Alizadeh-Choobari et al., 2014; Proestakis et al., 2018). It is clear that the maximal emission and loading of dust aerosol over the TPS appeared in dust sources such as the TD and the ThD and their adjacent areas during spring (March-May, MAM) or summer (June-August, JJA) while decreasing during autumn (September-November, SON) and winter (December-February, DJF). The peak center of DOD over the TD was not changed for all seasons while that of the ThD was moving westward from MAM to JJA when the South Asian Monsoon (SAM) is the onset and intensified. However, the recalculated DOD in this study was smaller than those in previous researches (Alizadeh-Choobari et al., 2014; Chen et al., 2017; Xu et al., 2018), especially in areas dominated by other aerosol species.

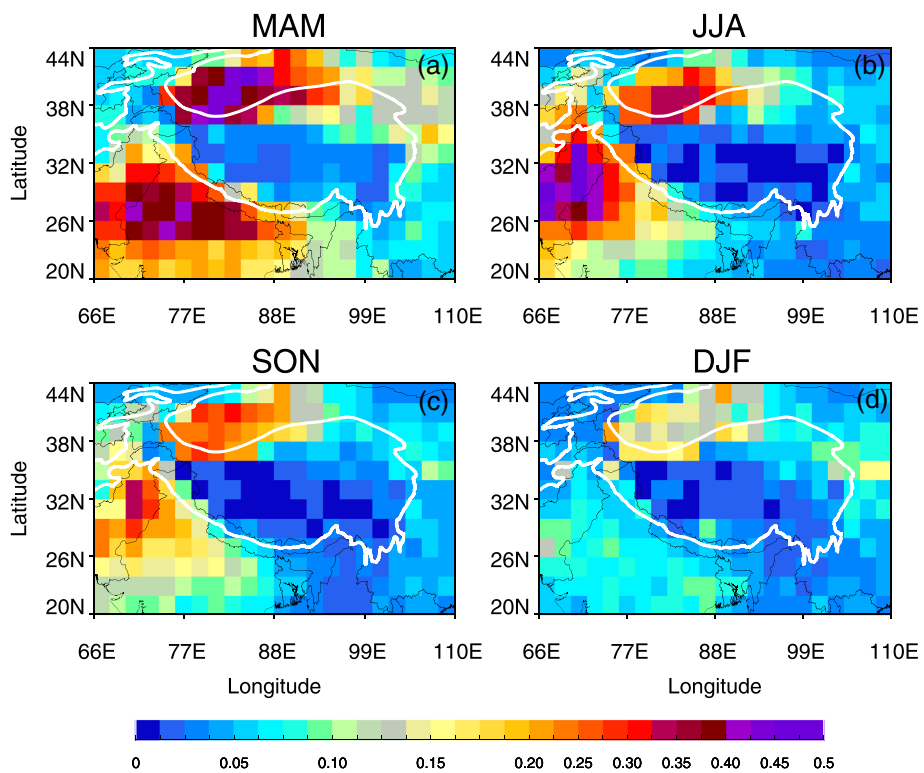


Figure 3. Seasonal distributions of the decadal mean of total DOD over the TPS during MAM, JJA, SON, and DJF. The TP is outlined with a solid white line at an altitude of 2,500 m.

the dust plume (Gautam et al., 2013). Additionally, the longitudinal cross-section of 93°E in the TP_R2 also shows a considerable vertical transport of the dust aerosol driven by the emission of abundant dust in the Qaidam Basin (Figures 4e and 4j).

3.2. Climatology of DRH

3.2.1. Horizontal Distribution

Figure 5 illustrates the seasonal spatial distributions of the decadal means of SW, LW, and net DRH averaged over the column of the atmosphere in the TPS. The result proved that the seasonal variation of SW, LW, and net DRH over the TPS was consistent with that of DOD as shown in Figure 3. Positive SW DRH indicates a higher heating rate under the dust condition as the dust aerosol absorbs SW radiation to heat the atmosphere (Figures 5a–5d) and may trigger an intense vertical transport of dust aerosol from neighboring sources (Lau et al., 2006). The warming centers mainly appeared in the TD, the ThD, and their adjacent transport areas. The peak value of the TD was approximately 9.0 K/month in MAM while 7.0 K/month in JJA for the ThD. The LW DRH showed mostly negative values, that is, cooler atmosphere under the dust condition, while the magnitude of the LW DRH was much smaller than that of the SW DRH (Figures 5e–5h). The peak center of LW cooling (about –1.5 K/month) mainly occurred at the TD in all seasons except for DJF due to infrequent dust aerosol.

Figures 5i–5l show the net DRH that reflects the comprehensive effects of dust aerosol on the atmospheric thermal structure. The result showed a positive warm effect. The peak centers were fully consistent with those of the SW DRH, 7 K/month over the TD in MAM, and 6.2 K/month over the ThD in JJA. The influence of dust aerosol over the TD on the atmospheric thermal structure in MAM or JJA was more pronounced than that over the ThD and adjacent transport regions. A larger warming effect of dust aerosol, 2.4 K/month in MAM and JJA, occurred at the Qaidam Basin in the TP_R2 region. The north of the TP_R1 also was affected by the positive net DRH (2–5 K/month), which is stronger than that in the south. The minimum net DRH was concentrated in the inland of the TP_R1 and TP_R3 due to lower dust aerosol emission and loading.

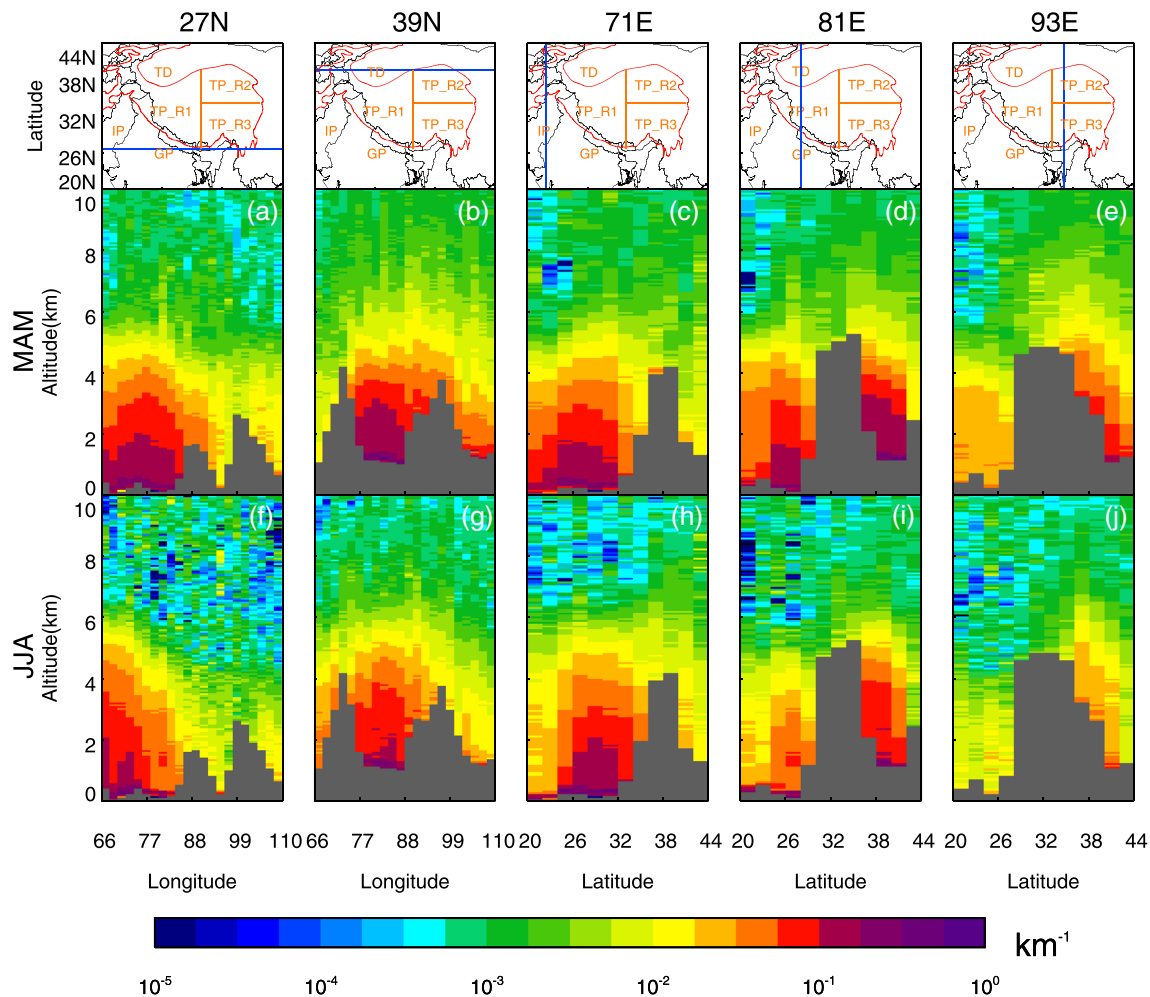


Figure 4. Vertical distributions of the decadal mean of the DEC at longitudinal (over 27°N and 39°N) and latitudinal (over 70°E, 81°E, and 93°E) cross-sections during MAM and JJA. The location of TP (orange) and cross-sections (blue) is indicated in the top panel.

3.2.2. Vertical Distribution

As in Figure 4, Figure 6 shows the vertical sections for the decadal mean DRH during MAM and JJA to clearly depict the vertical distribution of the DRH. Similar to the SE layer of dust aerosol, the maxima of the DRH appeared near the surface, and the DRH decreased with an increase in elevated height and transport range. The near-surface peaks of the DRH mainly occurred at the TD and the ThD and their adjacent transport regions. In particular, the DRH reached 22 K/month and even up to 42 K/month in MAM on the sections of 39°N and 81°E (Figures 6b and 6d) in the TD. A warming layer of DRH > 16 K/month was confined below 3.5 km in the TD during MAM while it occurred near the surface in the ThD during MAM (Figures 6a and 6c) and JJA (Figures 6f and 6h). A warming layer of DRH > 8 K/month was extended to 4 km in the TD during MAM and JJA while only 3 km in the GP during MAM and in the IP during JJA. Along with the eastward transport of dust aerosol over the TD, the DRH in MAM over Hexi Corridor (Figure 6b) was considerable, up to 6 K/month that is comparable to that of the Qaidam Basin (Figure 6e). On the northern slope of the TP (Figures 6d and 6i), we found a remarkable DRH warmer than that on the southern slope. Overall, the influence of DRH on the atmospheric thermal structure over the TD and TP was pronounced than that over the ThD in MAM or JJA.

The mean vertical profiles of the DRH for the six subregions were calculated to clearly understand the vertical distribution of DRH over the different subregions of the TPS as shown in Figure 7. On a regional average, the DRH decreased significantly with an increase in transport height and a decrease in DEC. During MAM, the maximum near-surface DRH over the TD (Figure 7a) reached up to 16.8 K/month which is

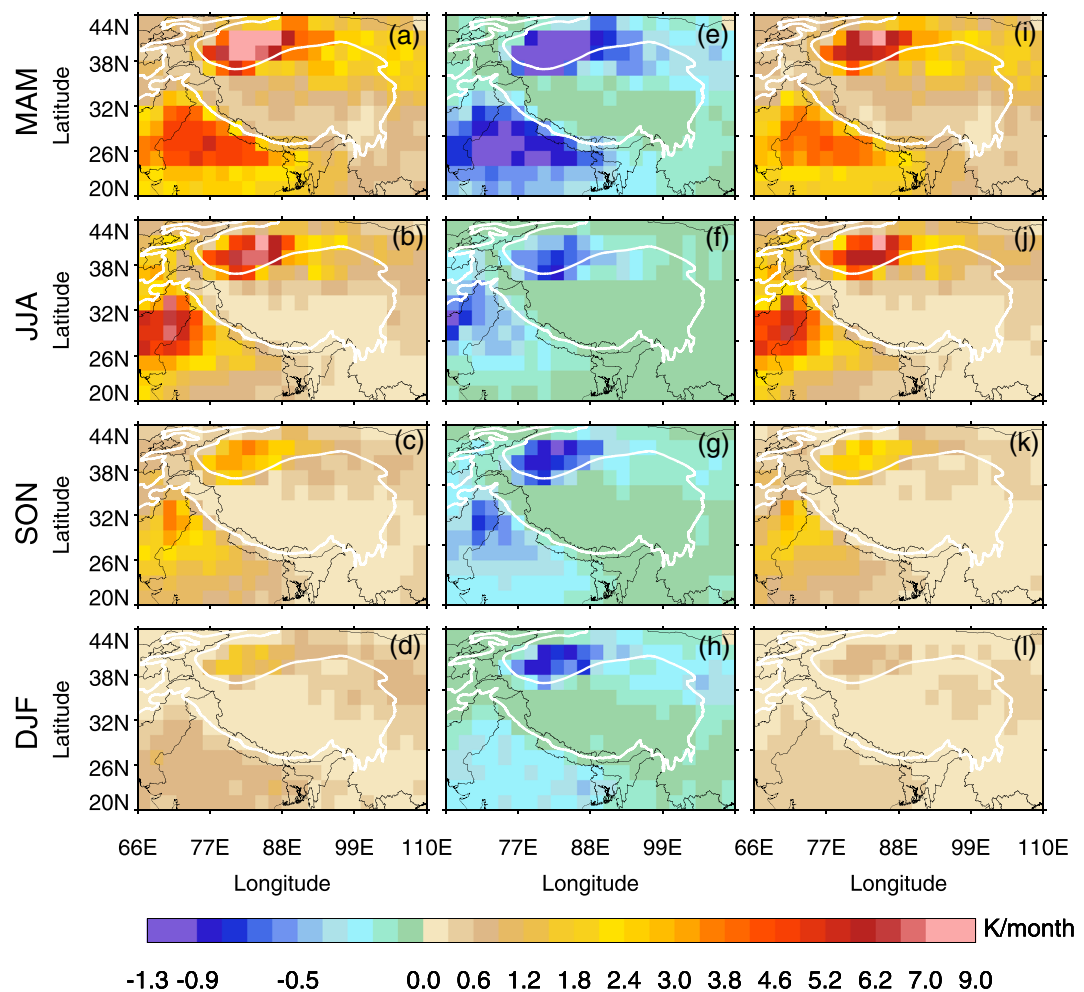


Figure 5. Seasonal spatial distributions of the decadal mean of column-averaged (a–d) SW, (e–h) LW, and (i–l) net DRF in the atmosphere over the TPS. The core region of TP is outlined with a white solid line at an altitude of 2,500 m.

almost 1.5 times that of the GP (10.8 K/month). The lapse speed of DRH with the height was slightly faster than that in the GP. Compared to the TD, in other words, a smaller near-surface DRH was observed in the GP during JJA while the fastest lapse speed of DRH with the height occurred (Figure 7b). These results may be induced by the heavy rainfalls under the SAM which interrupts the SE dust layer to rise to higher elevations. For the IP (Figure 7c), the DRH in JJA was stronger than that in MAM and the maximum DRH occurred at a height of 2 km, which may be related to the westward movement of the DOD peak center after the onset and intensification of the SAM. It is also noteworthy that the DRHs of 1 K/month in TD were extended to ~6 km while to a height of 5 km in the GP and the IP. For the TP, the maximum near-surface DRH occurred at the TP_R2 during MAM mainly due to the dust emission from the Qaidam Basin, which reached up to 4.7 K/month. For the TP_R1, the DRH profiles were similar to those of the TP_R2 in JJA with the maximum near-surface DRH of ~2.8 K/month. These positive DRHs (i.e., warming effects of the dust aerosol) indicate that the dust aerosol plays an important role in increasing the heating in the atmosphere. Particularly, an increase in the heating rate near the surface can accelerate the snow melting. Furthermore, the TPS may be susceptible to climate change due to the warming effects of the dust aerosol (Cheng & Wu, 2007). Therefore, the smaller DRH in the TP still needs to take into consideration.

3.3. Decadal Evolution of DRH

Although the decadal average of DRH in the TPS can well reflect the effect of dust aerosol on the atmospheric thermal structure, it shows only the mean movements over a decade. Therefore, this study

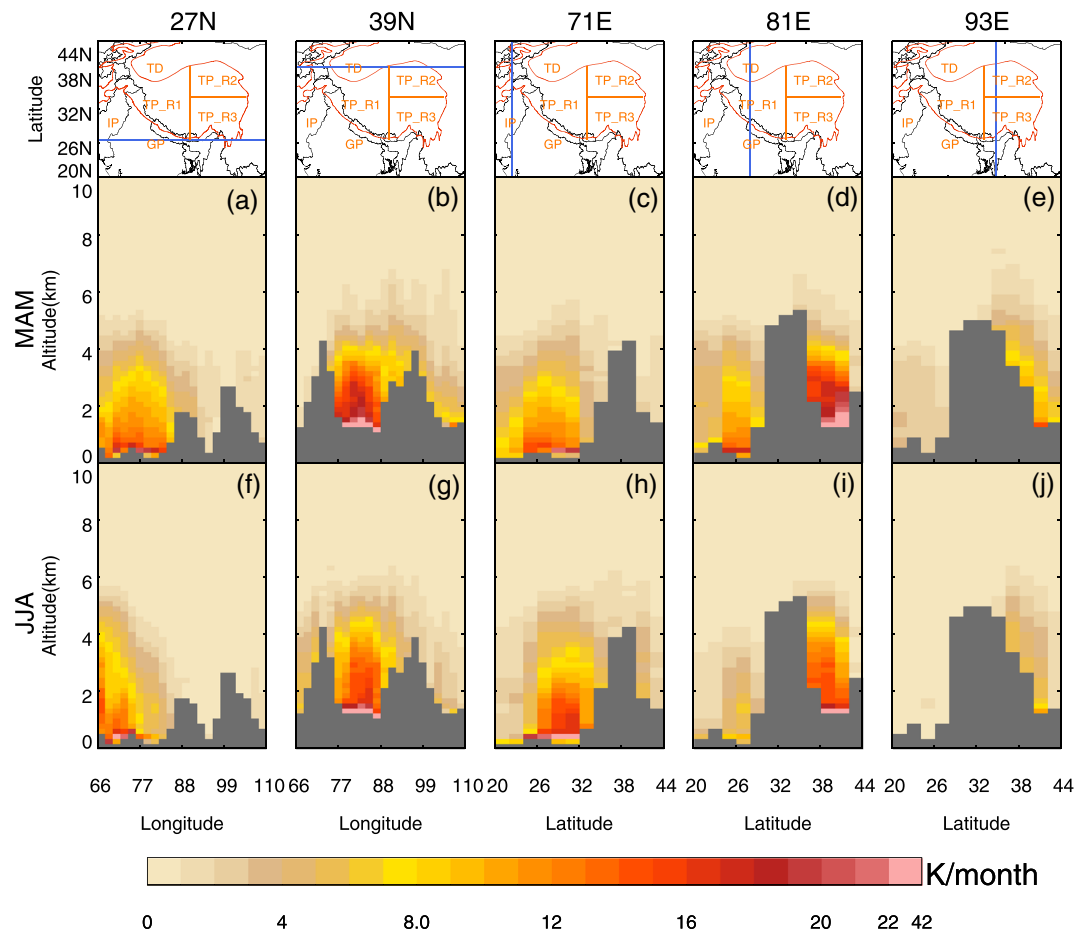


Figure 6. Same as in Figure 4, but for the net DRH.

investigated the historical evolution of DRH in the past decade, especially for the warming anomaly. Figure 8 shows the monthly DRHs (column-averaged) over six subregions from 2007 to 2016. The highest DRHs in the TD, the GP, and the TP appeared mostly from March to May, except for in the IP (from May to August) highly affected by the onset and intensification of the SAM. It is evident that the DRHs vary with month and subregions, that is, a considerable intermonth and interannual variability. This result is closely related to the frequency and intensity of dust events triggered by different atmospheric circulations. For example, the DRHs in August 2007 and 2012 were as high as 7–9 K/month in the TD and the IP and 1.5–2.5 K/month in the TP_R1, respectively, which are nearly twice higher than that of decadal average during the same period at the subregion. Such a result means that the DRH of the TP_R1 is likely affected by the dust aerosol transported from the TD and the IP. In addition, the superposition of dust aerosols sourced from the Qaidam Basin and the TD may contribute to a higher intermonth variability of the DRH in the TP_R2. Overall, the evolution of the DRH for the subregions further highlights the impacts of the dust aerosol from the TPS on the atmospheric thermal structure over the TP except for over the TP_R3.

3.4. Uncertainties in the DRH

Although the high-quality satellite data sets have been fed into the model in this study to minimize modeling errors from dust vertical extinction profile, surface albedo, and atmospheric parameters, there are inevitable uncertainties in estimating the DRH related to optical properties (He et al., 2017). In particular, the assumption of the transported dust mode may introduce an error for the SSA with a greater difference among the four dust modes in OPAC (Table 2). Che, Xia, et al. (2019) reported the SSA of mineral dust varied with locations and observation periods. Liu et al. (2011) observed the SSA (~0.87) during the dust period. Besides, the

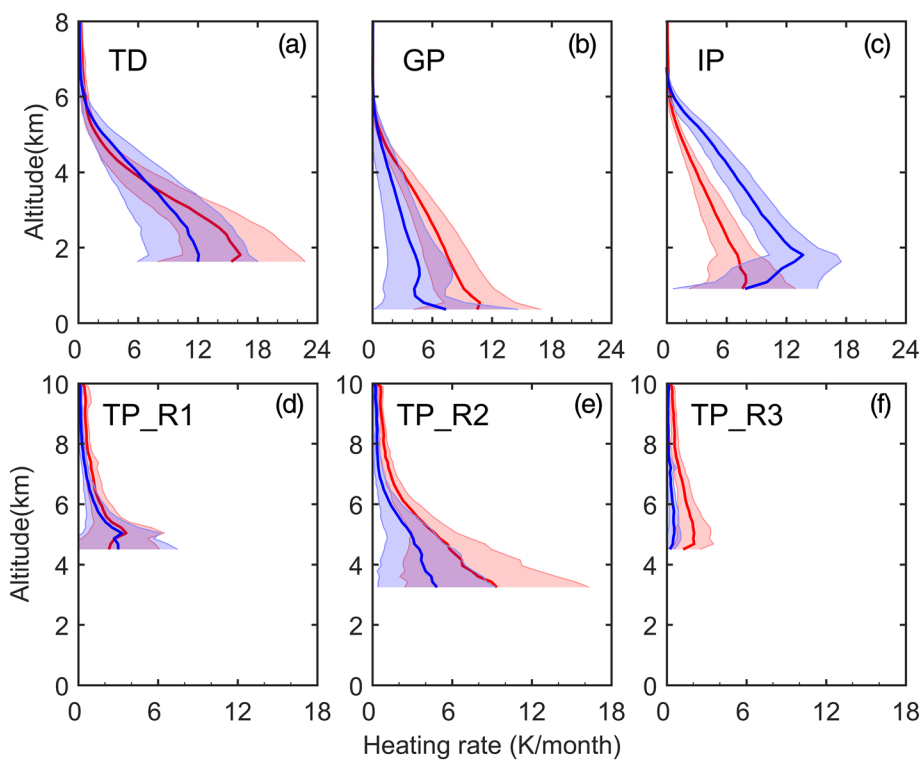


Figure 7. Vertical profiles of DRH over (a) TD, (b) GP, (c) IP, (d) TP_R1, (e) TP_R2, and (f) TP_R3 during MAM (red) and JJA (blue). The shading represents the standard deviation.

observation study of an Aerosol Robotic Network estimated the maximum SW spectral weighted SSA of the dust aerosol (0.94) over the TD (Dubovik et al., 2002; Kaskaoutis et al., 2012), which is 6% larger than that of transported dust (0.89). Thus, the uncertainty range in the SSA was estimated to be $\pm 6\%$ as in previous studies (Dubovik et al., 2002; Kaskaoutis et al., 2012). In addition, a fixed value of LR (44 in this study)

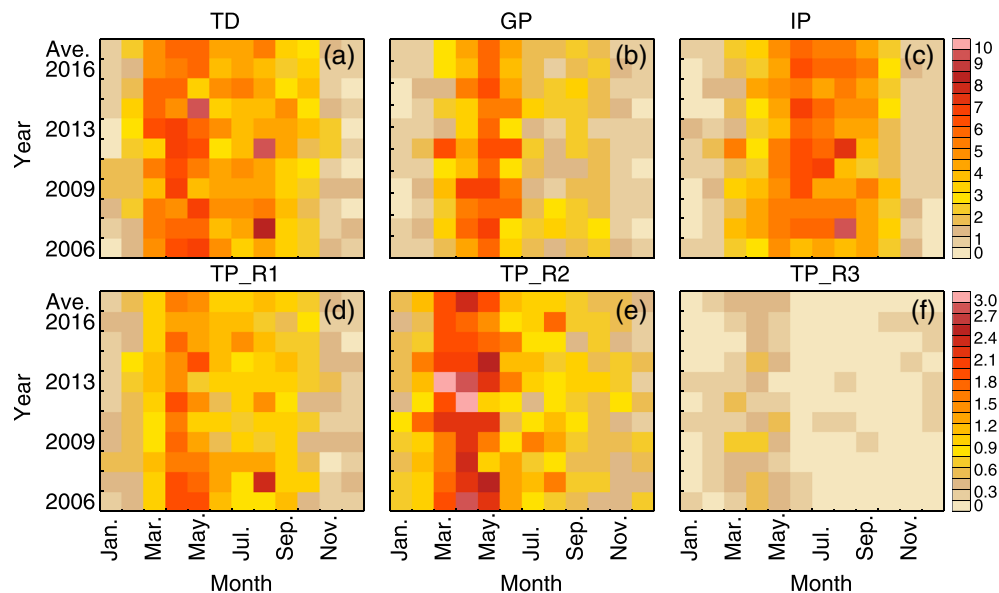


Figure 8. The evolution of monthly column-averaged DRH over (a) TD, (b) GP, (c) IP, (d) TP_R1, (e) TP_R2, and (f) TP_R3.

Table 3

The Absolute (Relative) Changes in the DRH (unit: K/month) Caused by the Ranges of the SSA and LR Over the TD, the IGP, and the TP Regions

	Region	MAM	JJA	SON	DJF
SSA ± 6%	TD	±1.68 (42%)	±1.28 (43%)	±0.67 (45%)	±0.32 (46%)
	IGP	±1.48 (44%)	±1.40 (43%)	±0.61 (43%)	±0.24 (45%)
	TP	±0.63 (42%)	±0.39 (43%)	±0.19 (45%)	±0.16 (47%)
LR ± 9	TD	±0.85 (20%)	±0.63 (20%)	±0.31 (21%)	±0.15 (21%)
	IGP	±0.64 (19%)	±0.62 (19%)	±0.30 (21%)	±0.11 (21%)
	TP	±0.30 (21%)	±0.19 (21%)	±0.09 (21%)	±0.07 (21%)

also may introduce a retrieval error of the dust extinction coefficient. This study also employed the range of LR (±9) based on the work of Omar et al. (2009) to estimate the uncertainty in the DRH. The absolute (relative) uncertainties of the DRH caused by the ranges of SSA (±6%) and LR (±9) are listed in Table 3 to investigate the impacts of dust aerosol loading. The maximum range occurred in MAM for all subregions, with the absolute (relative) value of ±1.68 (42%), ±1.48 (44%), and ±0.63 (42%) K/month over the TD, the IGP, and the TP, respectively. Same as for the SSA, the maximum ranges of the DRH caused by a change in LR also occurred in MAM, ±0.85 (20%), ±0.64 (19%), and ±0.30 (21%) K/month over the TD, the IGP, and the TP, respectively. Given that a certain level of uncertainty in the optical properties was introduced, it is demonstrated that the dust aerosol contributes to the warming effects on the atmospheric thermal structure especially for that near the surface.

4. Conclusions and Discussion

In this study, the decadal climatology of the DRH in the atmosphere over the TPS was investigated based on the radiative heating rate simulated by the SBDART model, multisource satellite observations and reanalysis data from 2007 to 2016. The separation of nondust aerosol and the average approach of single aerosol species were used to ensure the accuracy of the climatological feature of the dust aerosol extinction coefficient. The results showed that the dust aerosol plays a crucial role in the atmospheric thermal structure by a net warm effect, that is, a larger SW warming rate than a LW cooling rate. The DRH showed a good agreement with dust loading that has considerable seasonal and spatial variability. The maximum DOD and DRH over the TPS mainly occurred during MAM at the deserts and their adjacent transport areas except for the IG highly affected by the onset and intensification of the SAM. The vertical distribution of the DRH was also consistent with the dust extinction coefficient profile. The maximum DRH appeared near the surface and then decreased with an increase in elevated height. The decadal mean of the DRH near the surface reached 16.8 K/month at the TD, 10.8 K/month at the Gangetic Plain in MAM, and 13.7 K/month at the Indus Plain in JJA, which are 3.6, 3.0, and 3.1 times higher than those of the column-averaged values, respectively. For the TP, the superposition of dust aerosols sourced from the Qaidam Basin and the surroundings considerably contributed to increasing the DRH. The decadal mean of the DRH near the surface in the Qaidam Basin reached 4.7 K/month in MAM and 2.8 K/month in JJA. A considerable intermonth and interannual variability in the DRH was also found, indicating that the dust aerosol from the TPS plays an important role in alterations in the atmospheric thermal structure over the TP.

The most important impact factors for the net DRH in the atmosphere are the aerosol optical depth, the SSA, and the vertical profile of dust aerosols (Huang et al., 2009). The enhanced detection technology of CALIPSO can not only provide more accurate profile information but also reduce the uncertainties in the DRH. While the assumption of the transported SSA and LR may introduce inevitable uncertainties in the DRH (Huang et al., 2009), the SSA may contribute more considerably to the uncertainties in the SW DRH (Dubovik et al., 2002; Wang et al., 2019). This study also evaluated the uncertainties in the estimated DRHs by introducing the ranges of SSA (±6%) and LR (±9) into the SBDART model. The results showed the largest uncertainties of the DRH occurred in MAM over the TD. Nevertheless, the warming patterns were still observed, indicating that the dust aerosol contributes to the warming effects on the atmospheric thermal structure especially for that near the surface. It is no doubt that the warming pattern of the DRH may affect the temperature anomaly in the atmosphere, land, and snow cover, which may influence the large-scale accelerated warming over the past few decades (Huang et al., 2012; Lau et al., 2010). The significant warming effect near the surface may also cause potential on snow melting, resulting in alterations in the water cycle in the TP and corresponding downstream area and further the northern hemisphere climate system (Immerzeel et al., 2010; Thompson et al., 2016). Therefore, we need to pay more attention to the effect of absorbing aerosols on the atmospheric thermal structure and snow melting as well as the light-absorbing impurities deposited in snow.

Data Availability Statement

CALIPSO data are processed from the NASA Langley Research Center Atmospheric Science Data Center (<http://eosweb.larc.nasa.gov/>). MERRA-2, MODIS, and OMI data are acquired from the NASA Giovanni online data system (<https://giovanni.gsfc.nasa.gov/giovanni/>), developed and maintained by the NASA GES DISC. The ERA-interim data are obtained from ECMWF Integrated Forecasting System (<https://www.ecmwf.int/en/forecasts/datasets/browse-reanalysis-datasets>).

Acknowledgments

This research is funded by the Strategic Priority Research Program, Chinese Academy of Sciences (XDA20060103), the Ministry of Science and Technology of China (2017YFC1501403), and the National Natural Science Foundation of China (41775022, 41521004, and 41430425). Support from NASA for making satellite data sets accessible in public is greatly acknowledged.

References

- Alizadeh-Choobari, O., Sturman, A., & Zawar-Reza, P. (2014). A global satellite view of the seasonal distribution of mineral dust and its correlation with atmospheric circulation. *Dynamics of Atmospheres and Oceans*, 68, 20–34. <https://doi.org/10.1016/j.dynatmoce.2014.67.002>
- Amiridis, V., Wandinger, U., Marinou, E., Giannakaki, E., Tsekeri, A., Basart, S., et al. (2013). Optimizing Saharan dust CALIPSO retrievals. *Atmospheric Chemistry and Physics Discussions*, 13(6), 14,749–14,795. <https://doi.org/10.5194/acpd-13-14749-2013>
- Campbell, J. R., Tackett, J. L., Reid, J. S., Zhang, J., Curtis, C. A., Hyer, E. J., et al. (2012). Evaluating nighttime CALIOP 0.532 μm aerosol optical depth and extinction coefficient retrievals. *Atmospheric Measurement Techniques*, 5(9), 2143–2160. <https://doi.org/10.5194/amt-5-2143-2012>
- Cao, J., Qin, D., Kang, E., & Li, Y. (2006). River discharge changes in the Qinghai-Tibet plateau. *Chinese Science Bulletin*, 51(5), 594–600. <https://doi.org/10.1007/s11434-006-0594-6>
- Che, H., Gui, K., Xia, X., Wang, Y., Holben, B. N., Goloub, P., et al. (2019). Large contribution of meteorological factors to inter-decadal changes in regional aerosol optical depth. *Atmospheric Chemistry and Physics*, 19(16), 10,497–10,523. <https://doi.org/10.5194/acp-19-10497-2019>
- Che, H., Xia, X., Zhao, H., Dubovik, O., Holben, B. N., Goloub, P., et al. (2019). Spatial distribution of aerosol microphysical and optical properties and direct radiative effect from the China aerosol remote sensing network. *Atmospheric Chemistry and Physics*, 19(18), 11,843–11,864. <https://doi.org/10.5194/acp-19-11843-2019>
- Che, H., Zhang, X. Y., Xia, X., Goloub, P., Holben, B., Zhao, H., et al. (2015). Ground-based aerosol climatology of China: Aerosol optical depths from the China aerosol remote sensing network (CARSNET) 2002–2013. *Atmospheric Chemistry and Physics*, 15(13), 7619–7652. <https://doi.org/10.5194/acp-15-7619-2015>
- Chen, S., Huang, J., Li, J., Jia, R., Jiang, N., Kang, L., et al. (2017). Comparison of dust emissions, transport, and deposition between the Taklimakan Desert and Gobi Desert from 2007 to 2011. *Science China Earth Sciences*, 60(7), 1338–1355. <https://doi.org/10.1007/s11430-016-9051-0>
- Chen, S., Huang, J., Zhao, C., Qian, Y., Leung, L. R., & Yang, B. (2013). Modeling the transport and radiative forcing of Taklimakan dust over the Tibetan Plateau: A case study in the summer of 2006. *Journal of Geophysical Research: Atmospheres*, 118, 797–812. <https://doi.org/10.1002/jgrd.50122>
- Chen, S., Zhao, C., Qian, Y., Leung, L. R., Huang, J., Huang, Z., et al. (2014). Regional modeling of dust mass balance and radiative forcing over East Asia using WRF-Chem. *Aeolian Research*, 15, 15–30. <https://doi.org/10.1016/j.aeolia.2014.02.001>
- Chen, Y., Li, W., Deng, H., Fang, G., & Li, Z. (2016). Changes in Central Asia's water tower: Past, present and future. *Science Reports*, 6, 35458. <https://doi.org/10.1038/srep35458>
- Cheng, G., & Wu, T. (2007). Responses of permafrost to climate change and their environmental significance, Qinghai-Tibet Plateau. *Journal of Geophysical Research*, 112, F02S03. <https://doi.org/10.1029/2006jf000631>
- Dubovik, O., Holben, B., Eck, T. F., Smirnov, A., Kaufman, Y. J., King, M. D., et al. (2002). Variability of absorption and optical properties of key aerosol types observed in worldwide locations. *Journal of the Atmospheric Sciences*, 59(3), 590–608. [https://doi.org/10.1175/1520-0469\(2002\)059<0590:VOAAOP>2.0.CO;2](https://doi.org/10.1175/1520-0469(2002)059<0590:VOAAOP>2.0.CO;2)
- Flanner, M. G., Zender, C. S., Hess, P. G., Mahowald, N. M., Painter, T. H., Ramanathan, V., & Rasch, P. J. (2009). Springtime warming and reduced snow cover from carbonaceous particles. *Atmospheric Chemistry and Physics*, 9(7), 2481–2497. <https://doi.org/10.5194/acp-9-2481-2009>
- Freudenthaler, V., Esselborn, M., Wiegner, M., Heese, B., Tesche, M., Ansmann, A., et al. (2017). Depolarization ratio profiling at several wavelengths in pure Saharan dust during SAMUM 2006. *Chemical and Physical Meteorology*, 61(1), 165–179. <https://doi.org/10.1111/j.1600-0889.2008.00396.x>
- Gautam, R., Hsu, N. C., Lau, W. K. M., & Yasunari, T. J. (2013). Satellite observations of desert dust-induced Himalayan snow darkening. *Geophysical Research Letters*, 40, 988–993. <https://doi.org/10.1002/grl.50226>
- Guo, J. P., Lou, M., Miao, Y., Wang, Y., Zeng, Z., Liu, H., et al. (2017). Trans-Pacific transport of dust aerosols from East Asia: Insights gained from multiple observations and modeling. *Environmental Pollution*, 230, 1030–1039. <https://doi.org/10.1016/j.envpol.2017.07.062>
- Hayasaka, T., Satake, S., Shimizu, A., Sugimoto, N., Matsui, I., Aoki, K., & Muraji, Y. (2007). Vertical distribution and optical properties of aerosols observed over Japan during the Atmospheric Brown Clouds–East Asia Regional Experiment 2005. *Journal of Geophysical Research*, 112, D22S35. <https://doi.org/10.1029/2006jd008086>
- Haynes, J. M., Vonder Haar, T. H., L'Ecuyer, T., & Henderson, D. (2013). Radiative heating characteristics of Earth's cloudy atmosphere from vertically resolved active sensors. *Geophysical Research Letters*, 40, 624–630. <https://doi.org/10.1002/grl.50145>
- He, L. J., Wang, L. C., Lin, A. W., Zhang, M., Bilal, M., & Tao, M. H. (2017). Aerosol optical properties and associated direct radiative forcing over the Yangtze River basin during 2001–2015. *Remote Sensing*, 9(7), 746–769. <https://doi.org/10.3390/rs9070746>
- Hess, M., Koepke, P., & Schulte, I. (1998). Optical Properties of Aerosols and Clouds: The Software Package OPAC. *Bulletin of the American Meteorological Society*, 79(5), 831–844. [https://doi.org/10.1175/1520-0477\(1998\)079<0831:opoaac>2.0.co;2](https://doi.org/10.1175/1520-0477(1998)079<0831:opoaac>2.0.co;2)
- Huang, J., Fu, Q., Su, J., Tang, Q., Minnis, P., Hu, Y., et al. (2009). Taklimakan dust aerosol radiative heating derived from CALIPSO observations using the Fu-Liou radiation model with CERES constraints. *Atmospheric Chemistry and Physics*, 9(12), 4011–4021. <https://doi.org/10.5194/acp-9-4011-2009>
- Huang, J., Ge, J., & Weng, F. (2007). Detection of Asia dust storms using multisensor satellite measurements. *Remote Sensing of Environment*, 110(2), 186–191. <https://doi.org/10.1016/j.rse.2007.02.022>

- Huang, J., Guan, X., & Ji, F. (2012). Enhanced cold-season warming in semi-arid regions. *Atmospheric Chemistry and Physics*, 12(12), 5391–5398. <https://doi.org/10.5194/acp-12-5391-2012>
- Huang, J., Minnis, P., Chen, B., Huang, Z., Liu, Z., Zhao, Q., et al. (2008). Long-range transport and vertical structure of Asian dust from CALIPSO and surface measurements during PACDEX. *Journal of Geophysical Research*, 113, D23212. <https://doi.org/10.1029/2008jd010620>
- Huang, J., Minnis, P., Lin, B., Wang, T., Yi, Y., Hu, Y., et al. (2006). Possible influences of Asian dust aerosols on cloud properties and radiative forcing observed from MODIS and CERES. *Geophysical Research Letters*, 33, L06824. <https://doi.org/10.1029/2005gl024724>
- Huang, J., Minnis, P., Yi, Y., Tang, Q., Wang, X., Hu, Y., et al. (2007). Summer dust aerosols detected from CALIPSO over the Tibetan Plateau. *Geophysical Research Letters*, 34, L18805. <https://doi.org/10.1029/2007gl029938>
- Huang, J., Wang, T., Wang, W., Li, Z., & Yan, H. (2014). Climate effects of dust aerosols over east Asian arid and semiarid regions. *Journal of Geophysical Research: Atmospheres*, 119, 11,398–11,416. <https://doi.org/10.1002/2014jd021796>
- Huang, J., Yu, H., Guan, X., Wang, G., & Guo, R. (2015). Accelerated dryland expansion under climate change. *Nature Climate Change*, 6(2), 166–171. <https://doi.org/10.1038/nclimate2837>
- Huang, Z., Qi, S., Zhou, T., Dong, Q., Ma, X., Zhang, S., et al. (2020). Investigation of aerosol absorption with dual-polarization lidar observations. *Optics Express*, 28(5), 7028–7035. <https://doi.org/10.1364/OE.390475>
- Immerzeel, W. W., Van Beek, L. P., & Bierkens, M. F. (2010). Climate change will affect the Asian water towers. *Science*, 328(5984), 1382–1385. <https://doi.org/10.1126/science.1183188>
- Jia, R., Liu, Y. Z., Chen, B., Zhang, Z. J., & Huang, J. P. (2015). Source and transportation of summer dust over the Tibetan Plateau. *Atmospheric Environment*, 123, 210–219. <https://doi.org/10.1016/j.atmosenv.2015.10.038>
- Johansson, E., Devasthale, A., Ecuyer, T., Ekman, A. M. L., & Tjernström, M. (2015). The vertical structure of cloud radiative heating over the Indian subcontinent during summer monsoon. *Atmospheric Chemistry and Physics*, 15(20), 11,557–11,570. <https://doi.org/10.5194/acp-15-11557-2015>
- Kang, S., Xu, Y., You, Q., Flügel, W.-A., Pepin, N., & Yao, T. (2010). Review of climate and cryospheric change in the Tibetan Plateau. *Environmental Research Letters*, 5, 015101. <https://doi.org/10.1088/1748-9326/5/1/015101>
- Kaskaoutis, D. G., Kahn, R. A., Gupta, P., Jayaraman, A., & Bartokas, A. (2012). Desert dust properties, modelling, and monitoring. *Advances in Meteorology*, 2012, 483632. <https://doi.org/10.1155/2012/483632>
- Kim, M.-H., Omar, A. H., Tackett, J. L., Vaughan, M. A., Winker, D. M., Trepte, C. R., et al. (2018). The CALIPSO version 4 automated aerosol classification and lidar ratio selection algorithm. *Atmospheric Measurement Techniques*, 11(11), 6107–6135. <https://doi.org/10.5194/amt-11-6107-2018>
- Konsta, D., Binietoglu, I., Gkikas, A., Solomos, S., Marinou, E., Proestakis, E., et al. (2018). Evaluation of the BSC-DREAM8b regional dust model using the 3D LIVAS-CALIPSO product. *Atmospheric Environment*, 195, 46–62. <https://doi.org/10.1016/j.atmosenv.2018.09.047>
- Lau, K. M., Kim, M. K., & Kim, K. M. (2006). Asian summer monsoon anomalies induced by aerosol direct forcing: The role of the Tibetan Plateau. *Climate Dynamics*, 26(7–8), 855–864. <https://doi.org/10.1007/s00382-006-0114-z>
- Lau, W. K. M., Kim, M. K., Kim, K. M., & Lee, W. S. (2010). Enhanced surface warming and accelerated snow melt in the Himalayas and Tibetan Plateau induced by absorbing aerosols. *Environmental Research Letters*, 5, 025204. <https://doi.org/10.1088/1748-9326/5/2/025204>
- Liu, D., Wang, Y., Wang, Z., & Zhou, J. (2012). The three-dimensional structure of transatlantic African dust transport: A new perspective from CALIPSO LIDAR measurements. *Advances in Meteorology*, 2012, 850704. <https://doi.org/10.1155/2012/850704>
- Liu, D., Wang, Z., Liu, Z., Winker, D., & Trepte, C. (2008). A height resolved global view of dust aerosols from the first year CALIPSO lidar measurements. *Journal of Geophysical Research*, 113, D16214. <https://doi.org/10.1029/2007jd009776>
- Liu, Y., Huang, J., Shi, G., Takamura, T., Khatri, P., Bi, J., et al. (2011). Aerosol optical properties and radiative effect determined from sky-radiometer over Loess Plateau of Northwest China. *Atmospheric Chemistry and Physics*, 11, 11,455–11,463. <https://doi.org/10.5194/acp-11-11455-2011>
- Liu, Y., Sato, Y., Jia, R., Xie, Y., Huang, J., & Nakajima, T. (2015). Modeling study on the transport of summer dust and anthropogenic aerosols over the Tibetan Plateau. *Atmospheric Chemistry and Physics*, 15(21), 12,581–12,594. <https://doi.org/10.5194/acp-15-12581-2015>
- Liu, Y. Z., Li, Y. H., Huang, J. P., Zhu, Q. Z., & Wang, S. S. (2020). Attribution of the Tibetan Plateau to northern drought. *National Science Review*, 7(3), 489–492. <https://doi.org/10.1093/nsr/nwz191>
- Liu, Z., Kar, J., Zeng, S., Tackett, J., Vaughan, M., Avery, M., et al. (2019). Discriminating between clouds and aerosols in the CALIOP version 4.1 data products. *Atmospheric Measurement Techniques*, 12(1), 703–734. <https://doi.org/10.5194/amt-12-703-2019>
- Liu, Z., Liu, D., Huang, J., Vaughan, M., Uno, I., Sugimoto, N., et al. (2008). Airborne dust distributions over the Tibetan Plateau and surrounding areas derived from the first year of CALIPSO lidar observations. *Atmospheric Chemistry and Physics*, 8(16), 5045–5060. <https://doi.org/10.5194/acp-8-5045-2008>
- Luo, T., Wang, Z., Zhang, D., Liu, X., Wang, Y., & Yuan, R. (2015). Global dust distribution from improved thin dust layer detection using A-train satellite lidar observations. *Geophysical Research Letters*, 42, 620–628. <https://doi.org/10.1002/2014gl062111>
- Ma, X., Huang, Z., Qi, S., Huang, J., Zhang, S., Dong, Q., & Wang, X. (2020). Ten-year global particulate mass concentration derived from space-borne CALIPSO lidar observations. *Science of the Total Environment*, 721, 137699. <https://doi.org/10.1016/j.scitotenv.2020.137699>
- Omar, A. H., Winker, D. M., Vaughan, M. A., Hu, Y., Trepte, C. R., Ferrare, R. A., et al. (2009). The CALIPSO automated aerosol classification and Lidar ratio selection algorithm. *Journal of Atmospheric and Oceanic Technology*, 26(10), 1994–2014. <https://doi.org/10.1175/2009jtecha1231.1>
- Painter, T. H., Skiles, S. M., Deems, J. S., Brandt, W. T., & Dozier, J. (2018). Variation in rising limb of Colorado River snowmelt runoff hydrograph controlled by dust radiative forcing in snow. *Geophysical Research Letters*, 45, 797–808. <https://doi.org/10.1002/2017GL075826>
- Peris-Ferrús, C., Gomez-Amo, J. L., Marcos, C., Freile-Aranda, M. D., Utrillas, M. P., & Martinez-Lozano, J. A. (2017). Heating rate profiles and radiative forcing due to a dust storm in the Western Mediterranean using satellite observations. *Atmospheric Environment*, 160, 142–153. <https://doi.org/10.1016/j.atmosenv.2017.04.023>
- Proestakis, E., Amiridis, V., Marinou, E., Georgoulias, A. K., Solomos, S., Kazadzis, S., et al. (2018). Nine-year spatial and temporal evolution of desert dust aerosols over south and East Asia as revealed by CALIOP. *Atmospheric Chemistry and Physics*, 18(2), 1337–1362. <https://doi.org/10.5194/acp-18-1337-2018>
- Pullen, A., Kapp, P., McCallister, A. T., Chang, H., Gehrels, G. E., Garzione, C. N., et al. (2011). Qaidam Basin and northern Tibetan Plateau as dust sources for the Chinese loess plateau and paleoclimatic implications. *Geology*, 39(11), 1031–1034. <https://doi.org/10.1130/g32296.1>
- Qiu, J. (2008). China: The third pole. *Nature*, 454(7203), 393–396. <https://doi.org/10.1038/454393a>

- Ricchiazzi, P., Yang, S., Gautier, C., & Sowle, D. (1998). SBDART: A research and teaching software tool for plane-parallel Radiative transfer in the Earth's atmosphere. *Bulletin of the American Meteorological Society*, 79(10), 2101–2114. [https://doi.org/10.1175/1520-0477\(1998\)079<2101:SDETPO>2.0.CO;2](https://doi.org/10.1175/1520-0477(1998)079<2101:SDETPO>2.0.CO;2)
- Shi, Z., Xie, X., Li, X., Yang, L., Xie, X., Lei, J., et al. (2019). Snow-darkening versus direct radiative effects of mineral dust aerosol on the Indian summer monsoon onset: Role of temperature change over dust sources. *Atmospheric Chemistry and Physics*, 19(3), 1605–1622. <https://doi.org/10.5194/acp-19-1605-2019>
- Sugimoto, N., Matsui, I., Shimizu, A., Uno, I., Asai, K., Endoh, T., & Nakajima, T. (2002). Observation of dust and anthropogenic aerosol plumes in the Northwest Pacific with a two-wavelength polarization lidar on board the research vessel Mirai. *Geophysical Research Letters*, 29(19), 1901. <https://doi.org/10.1029/2002gl015112>
- Thompson, L. G., Mosley-Thompson, E., & Yang, X. (2016). 6th third pole environment workshop, US Third Pole Environment Office, Byrd Polar and Climate Research Center.
- Uno, I., Eguchi, K., Yumimoto, K., Takemura, T., Shimizu, A., Uematsu, M., et al. (2009). Asian dust transported one full circuit around the globe. *Nature Geoscience*, 2(8), 557–560. <https://doi.org/10.1038/ngeo583>
- Wake, C. P., Mayewski, P. A., Li, Z., Han, J., & Qin, D. (1994). Modern eolian dust deposition in Central Asia. *Chemical and Physical Meteorology*, 46(3), 220–233. <https://doi.org/10.1034/j.1600-0889.1994.t01-2-00005.x>
- Wang, M., Su, J., Li, X., Wang, C., & Ge, J. (2019). Parameterization of the single-scattering properties of dust aerosols in radiative flux calculations. *Atmosphere*, 10, 728. <https://doi.org/10.3390/atmos10120728>
- Wang, T., Chen, Y., Gan, Z., Han, Y., Li, J., & Huang, J. (2020). Assessment of dominating aerosol properties and their long-term trend in the pan-third pole region: A study with 10-year multi-sensor measurements. *Atmospheric Environment*, 239, 117738. <https://doi.org/10.1016/j.atmosenv.2020.117738>
- Wang, T. H., & Huang, J. P. (2009). A method for estimating optical properties of dusty cloud. *Chinese Optics Letters*, 7(5), 368–372. <https://doi.org/10.3788/Col20090705.0368>
- Winker, D. M., Tackett, J. L., Getzewich, B. J., Liu, Z., Vaughan, M. A., & Rogers, R. R. (2013). The global 3-D distribution of tropospheric aerosols as characterized by CALIOP. *Atmospheric Chemistry and Physics*, 13(6), 3345–3361. <https://doi.org/10.5194/acp-13-3345-2013>
- Wonsick, M. M., Pinker, R. T., & Ma, Y. (2014). Investigation of the “elevated heat pump” hypothesis of the Asian monsoon using satellite observations. *Atmospheric Chemistry and Physics*, 14(16), 8749–8761. <https://doi.org/10.5194/acp-14-8749-2014>
- Xu, C., Ma, Y., Yang, K., & You, C. (2018). Tibetan Plateau impacts on global dust transport in the upper troposphere. *Journal of Climate*, 31(12), 4745–4756. <https://doi.org/10.1175/JCLI-D-17-0313.1>
- Xu, C., Ma, Y. M., Panday, A., Cong, Z. Y., Yang, K., Zhu, Z. K., et al. (2014). Similarities and differences of aerosol optical properties between southern and northern sides of the Himalayas. *Atmospheric Chemistry and Physics*, 14(6), 3133–3149. <https://doi.org/10.5194/acp-14-3133-2014>
- Xu, C., Ma, Y. M., You, C., & Zhu, Z. K. (2015). The regional distribution characteristics of aerosol optical depth over the Tibetan Plateau. *Atmospheric Chemistry and Physics*, 15(20), 12,065–12,078. <https://doi.org/10.5194/acp-15-12065-2015>
- Yan, H., & Wang, T. (2020). Ten years of aerosol effects on single-layer overcast clouds over the US southern Great Plains and the China loess plateau. *Advances in Meteorology*, 2020, 6719160. <https://doi.org/10.1155/2020/6719160>
- Yao, T., Thompson, L. G., Mosbrugger, V., Zhang, F., Ma, Y., Luo, T., et al. (2012). Third pole environment (TPE). *Environment and Development*, 3, 52–64. <https://doi.org/10.1016/j.envdev.2012.04.002>
- Yao, T., Xue, Y., Chen, D., Chen, F., Thompson, L., Cui, P., et al. (2019). Recent third pole's rapid warming accompanies cryospheric melt and water cycle intensification and interactions between monsoon and environment: Multidisciplinary approach with observations, modeling, and analysis. *Bulletin of the American Meteorological Society*, 100(3), 423–444. <https://doi.org/10.1175/bams-d-17-0057.1>
- Yao, T. D., Wang, Y. Q., Liu, S. Y., Pu, J. C., Shen, Y. P., & Lu, A. X. (2004). Recent glacial retreat in high Asia in China and its impact on water resource in Northwest China. *Science China Series D*, 47(12), 1065–1075. <https://doi.org/10.1360/03yd0256>
- Yasunari, T. J., Koster, R. D., Lau, W. K. M., & Kim, K. M. (2015). Impact of snow darkening via dust, black carbon, and organic carbon on boreal spring climate in the earth system. *Journal of Geophysical Research: Atmospheres*, 120, 5485–5503. <https://doi.org/10.1002/2014jd022977>
- Yu, H., Chin, M., Bian, H., Yuan, T., Prospero, J. M., Omar, A. H., et al. (2015). Quantification of trans-Atlantic dust transport from seven-year (2007–2013) record of CALIPSO lidar measurements. *Remote Sensing of Environment*, 159, 232–249. <https://doi.org/10.1016/j.rse.2014.12.010>
- Yu, H., Chin, M., Winker, D. M., Omar, A. H., Liu, Z., Kittaka, C., & Diehl, T. (2010). Global view of aerosol vertical distributions from CALIPSO lidar measurements and GOCART simulations: Regional and seasonal variations. *Journal of Geophysical Research*, 115, D00H30. <https://doi.org/10.1029/2009jd013364>
- Zhou, L., Zhu, J., Zou, H., Ma, S., Li, P., Zhang, Y., & Huo, C. (2014). Atmospheric moisture distribution and transport over the Tibetan Plateau and the impacts of the south Asian summer monsoon. *Acta Meteorologica Sinica*, 27(6), 819–831. <https://doi.org/10.1007/s13351-013-0603-z>